DirFis: A hybrid silicon and PPAC detector array for direct reaction and fission coincidence measurements[*]

S.X. Zhu,[1] H.M. Jia,[1, †] C.J. Lin,[1, 2, ‡] J. Feng,[1] Y.J. Qiu,[1] S.L. Liu,[1] Y. Yang,[1] L. Yang,[1]
N.R. Ma,[1] F. Yang,[1] P.W. Wen,[1] T.P. Luo,[1] C. Chang,[1] H.R. Duan,[1] and H.Q. Zhang[1]
[1]*Department of Nuclear Physics, China Institute of Atomic Energy, Beijing 102413, China*
[2]*College of Physics and Technology, Guangxi Normal University, Guilin 541004, China*

To further investigate heavy-ion reaction mechanisms and the fission of actinide nuclei using the surrogate reaction method, a compact and efficient hybrid detector array for coincidence measurements of beam-like particles and fission fragments has been developed and tested online. This detector array consists of four silicon strip detector telescopes and two parallel-plate avalanche counters. For the near-barrier ^{7}Li + ^{238}U reaction, the fission fragments correlated with the beam-like ^{6}He particles originating from the transfer reaction were confirmed by analyzing the folding angle. The fission barrier height for the short-lived actinide nucleus ^{239}Np, produced in the $1p$ stripping channel, was extracted from its fission probability. The deduced value is in good agreement with the existing literature data.

Keywords: Hybrid detector array; Coincidence measurement; Transfer-induced fission; Fission barrier height; Fission fragment folding angle

I. INTRODUCTION

Nuclear reactions with heavy-ions at energies around the Coulomb barrier are of great significance for studying the interplay between nuclear structure and reaction dynamics. Weakly bound nucleus induced reactions, owing to their low separation energy thresholds [1] and cluster structures [2–4], exhibit complicated reaction mechanisms of breakup, incomplete fusion and cluster transfers in the near-barrier energy region. Over the past three decades, to thoroughly investigate the reaction mechanisms induced by weakly bound nuclei, many silicon strip detector arrays have been developed worldwide, such as MUST [5], LEDA [6], EXPADES [7], GLORIA [8], MITA [9] and STARE [10]. These detector arrays have greatly advanced the experimental research in this field.

However, several key issues in weakly bound nuclear systems still remain. Among them, the competition between breakup-incomplete fusion and transfer reactions, as well as the controversy over their relative contributions, has persisted for decades [11–16]. From an experimental perspective, since both breakup and transfer processes can produce the same beam-like particles (BLP), it is difficult to effectively distinguish between these two reaction mechanisms from an inclusive measurement. To address this, various experimental techniques have been developed over the years, including α decay measurements of target-like particles (TLP) [13, 15, 17], coincidence of BLP-γ [12, 16, 18–25], and BLP-fission fragment (FF) [26–28]. Compared to the coincidence measurements with α-decay or γ, which suffer from the half-life restriction or uncertainty in γ-decay branching ratio, the coincidence with FF has the advantage of covering a wide excitation energy range and yielding more reliable quantitative results [26, 28].

In addition to reaction mechanisms, fission-related studies are also of considerable interest. Nuclear fission, since its discovery about 90 years ago, remains one of the most challenging subjects in nuclear physics both experimentally [29–31] and theoretically [29, 32, 33]. Fission is also widely utilized in power reactors, which currently generate approximately 11% of the world's electricity [34]. It also holds significant application value in interdisciplinary fields such as nuclear astrophysics, nuclear medicine and environment [35]. The fission barrier height, introduced by Bohr and Wheeler [36], is one of the most fundamental quantities describing nuclear fission. To date, information on fission barriers in actinide nuclei has been mainly obtained through direct neutron induced fission and indirect transfer surrogate methods, including (t, d) [37], (d, p) [38–40], (t, p) [41, 42], (^{3}He$, d)$ [41–43] and (^{18}O,x) [44] reactions. Compared to neutron-induced reactions, transfer-induced fission offers a significant advantage of studying short-lived unstable nuclides, wherein the natural decay not only makes sample handling difficult but also generates intense background signals in measurements, posing substantial challenges for neutron-induced reaction studies.

To further investigate reaction mechanisms and fission related physics, a compact hybrid setup, named DirFis, consisting of silicon strip detectors and parallel-plate avalanche counters (PPACs) has been built and tested. The importance of ^{239}Np fission, which is a key intermediate nuclide in the nuclear fuel cycle and has accumulated extensive experimental data on its fission barrier [42–44], makes it a suitable candidate for validating the reliability of the present detector array.

In this work, coincidence measurements between fission fragments and beam-like particles were performed for the weakly bound ^{7}Li $+^{238}$ U system at the near-barrier energy E_{Lab} = 36.8 MeV. The variation of the fission probability

---

[*] Supported by the National Key R&D Program of China(Contract Nos. 2023YFA1606402 and 2022FYA1602301), the National Natural Science Foundation of China (Grant Nos. 12235020, 12275360, U2167204 and 12175314), Platform Stable Support Projects of CNNC-PTWZ-202506 and the Continuous-Support Basic Scientific Research Project.

[†] Corresponding author, jiahm@cnncmail.cn
[‡] Corresponding author, cjlin@ciae.ac.cn

of the target-like nucleus ^{239}Np with excitation energy was determined from the emitting BLP ^{6}He originating from $1p$ stripping, and the fission barrier height of ^{239}Np was extracted. The design of the hybrid detector array is described in Section II. Section III presents the offline test results. Section IV discusses the in beam test results followed by the summary in Section V.

II. THE HYBRID DETECTOR ARRAY

The detector array is illustrated in Fig. 1, where the arrow indicates the beam direction. Four ΔE-E silicon strip detector telescopes Si$_{0-3}$ were placed at backward angles of 112° and 155° relative to the beam direction to identify the beam-like particles. Each telescope consists of three layers of 50×50 mm^2 silicon detectors: the first layer is a single-sided silicon strip detector (SSSD) with a nominal thickness of 20 μm, the second layer is an SSSD with a thickness of 300 μm, and the third layer is a quadrant silicon detector (QSD) with a thickness of 1000 μm. Each SSSD is segmented into 16 strips with the strip orientations of the first two layers perpendicular to each other, forming 256 pixels with areas of 3.0×3.0 mm^2. All the SSSDs and QSDs were manufactured by the Micron Semiconductor Ltd [45]. The first and second layers are used to detect heavier particles such as Li and He isotopes, while the second and third layers are used to detect lighter particles like p, d and t.

The distances from the target to the detectors are 162.7 mm for Si$_{0,1}$ and 167.5 mm for Si$_{2,3}$, with an angular coverage of $\pm0.55°$ per pixel. The total solid angle covered by the four silicon strip detector telescopes is 0.1π. A 0.5 μm thick Mylar film was installed in front of each silicon telescope to minimize the influence of low-energy electrons on the first layer silicon detectors during online experiments. All silicon detectors were coupled with self-made integrated charge-sensitive preamplifiers [46] in vacuum, working in a cooled condition to optimize the energy resolution and ensure performance stability. These preamplifiers have been applied in several experiments and exhibit excellent and stable performance [10, 47–50].

Two PPACs, each with an active area of 296×200 mm^2, were employed to detect the fission fragments. Both the entrance and exit windows are 2.0-μm-thick Mylar film. Both PPACs adopt a conventional three-electrode structure, consisting of an X anode, a cathode, and a Y anode. The distance from the anode plane to the cathode plane is 3.0 mm. The anode wires are 20-μm-diameter gold-plated tungsten wires with a spacing of 1.0 mm between every two wires and coupled to delay lines. Two adjacent wires in the X direction were read out together as one channel, while three adjacent wires in the Y direction were read out together as one. Therefore, each PPAC has 146 position information in X direction and 66 position information in Y direction. More detailed description of the PPAC can be found in [51]. The electronics system was used to acquire TDC time signals and ADC energy signals. To maximize the detection efficiency with appropriate counting rates, the two PPACs were positioned at 57° and 96° respectively, based on the folding angle distribution. The forward-angle PPAC detector (PPAC$_{\mathrm{F}}$) was placed at a distance of 187 mm from the target center, while the backward-angle one (PPAC$_{\mathrm{B}}$) was placed at a distance of 152 mm. The covered polar angle θ ranges from 20.2° to 96.2° and from 52.5° to 140.2°, respectively. The total solid angle covered by the two PPAC detectors (Ω_{PPAC}) amounts to 0.85π.

Four PIN silicon detectors were placed at fixed forward angles of $\pm15°$ and $\pm20°$ relative to the beam direction as monitors. They were used to monitor the beam direction and spot size, as well as to normalize reaction cross sections via Rutherford scattering.

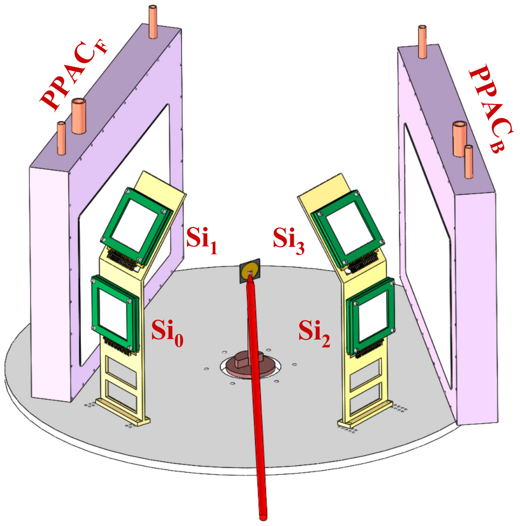

Fig. 1. (Color online) Schematic view of the hybrid detector array, mainly consisting of four ΔE-E silicon strip detector telescopes and two PPAC detectors. The long arrow indicates the beam direction.

III. OFFLINE TESTS

Good energy and position resolutions are essential for kinematic measurements, which are crucial for characterizing the reaction processes of weakly-bound nuclei. Therefore, offline performance tests were conducted using a three-component α source for the silicon detectors and a ^{252}Cf fission source for the PPAC detectors, in order to obtain their performance and determine the optimal operating conditions.

A. Silicon detector performance with a three-component α source

The three-component α source consists of ^{239}Pu, ^{241}Am and ^{244}Cm. The 20-μm thick silicon layer is too thin for complete energy deposition of these αs, and the α particles will hit the 300-μm layer. A typical E_1-E_2 energy spectrum of α

particles detected in a pixel of Si_0 is shown in Fig. 2(a). The large variation in the energy loss observed in the first silicon layer is mainly attributed to the thickness non-uniformity of the thin silicon detector. The total energy E_1+E_2 spectrum is shown in Fig. 2(b). The three separate groups correspond to the three components. A Gaussian fit to the peak of 5.486 MeV α particles emitted from ^{241}Am yields an energy resolution of $\sim$1.2% for the total energy E_1+E_2, as shown by the solid line.

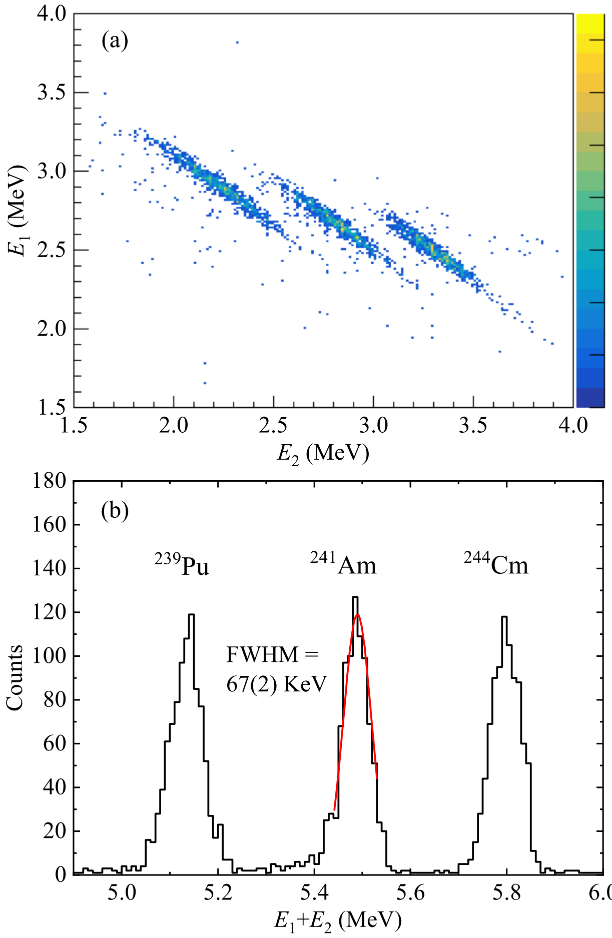

Fig. 2. (Color online) Performance of the first two layers of Si_0 detector telescope tested with a three-component α source. (a) E_1-E_2 spectrum of the α particles from the decay of the three-component α source. (b) Total energy E_1+E_2 spectrum. The Gaussian fitting (solid line) for the middle group gives an energy resolution of $\sim$1.2% for the 5.486 MeV α peak.

B. PPAC position resolution with a ^{252}Cf source

The position resolution of the PPAC detector mainly depends on the nature of the incident ions, the working gas, and the applied high voltage. Isobutane gas with a purity of 99.99% was used as the working gas of PPAC detectors. The optimal operating conditions were achieved at a pressure of 4.5 Torr and a high voltage of -550 V for both PPACs. A typical result obtained for ^{252}Cf fission fragments under these conditions is shown in Fig. 3. Panels (a) and (b) show the typical position resolution spectra of $\mathrm{PPAC_B}$ in the X and Y directions, respectively. The position calibration was obtained from the linear proportional relationship between the time signal difference and the geometric position. From Gaussian fits to the position peaks, the average FWHM of the detector in the X and Y direction are 0.94 ± 0.03 mm and $2.21{\pm}0.08$ mm, respectively. It can be seen that good position resolution was achieved from both the X and Y directions.

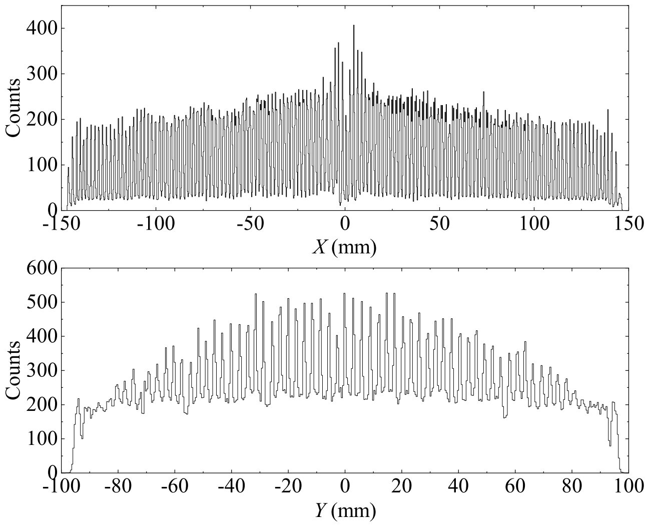

Fig. 3. Performance of the $\mathrm{PPAC_B}$ detector tested with a ^{252}Cf source. (a) Position spectrum in the X direction. (b) Position spectrum in the Y direction.

IV. IN BEAM TEST

The experiment was conducted at the HI-13 tandem accelerator of the China Institute of Atomic Energy. The ^{238}U target was selected considering the high fissility of its target-like particles after transfer reactions. The ^{238}U target with a thickness of 370 μg/cm^2 was sandwiched between a 33 nm aluminum foil and a 50 μg/cm^2 carbon backing. The target was fixed at the center of the hybrid detector array with a normal angle of 30° relative to the beam direction, in order to minimize the energy loss of fission fragments in the target and the dead area caused by the target frame. The reaction energy for ^{7}Li + ^{238}U is E_{lab} = 36.8 MeV. The irradiation time was 20 hours with a beam intensity of $\sim$10 enA. The low-energy ^{79}Br + ^{238}U elastic scattering was selected to calibrate the geometrical alignment of the two PPACs.

A. Calibration of the PPACs by using ^{79}Br + ^{238}U elastic scattering

Elastic scattering of ^{79}Br + ^{238}U at a beam energy 170 MeV was used to calibrate the geometry of the two PPACs. The obtained folding angle distribution of the ^{79}Br + ^{238}U elastic scattering is shown in Fig. 4. The red solid line represents the scattered beam component, while the green dashed line represents the recoiled target nucleus component. The good agreement of the experimental data with the kinematic calculations confirms the good position calibration and installation geometry.

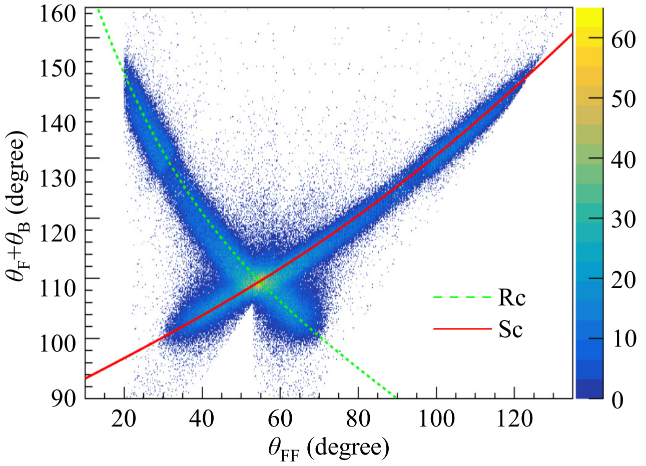

Fig. 4. (Color online) The folding angle distribution for the ^{79}Br + ^{238}U elastic scattering at 170 MeV. The X-axis shows the θ coverage angle of the PPACs, and the Y-axis shows the folding angle of the two simultaneously emitted fragments. The lines represent kinematic calculations, where the red solid line corresponds to the scattered beam component (Sc), and the green dashed line corresponds to the recoiled target nucleus component (Rc).

B. Identification of beam-like particles

A typical inclusive ΔE-E particle identification spectrum measured by the silicon strip detector telescope Si$_0$ in ^{7}Li + ^{238}U at $E_{\rm lab}$ = 36.8 MeV and $\theta_{\rm lab}$ = 155° is shown in Fig. 5. In Fig. 5(a), E_1 is the energy loss in the first layer, and E_1+E_2 is the sum of the energy loss in the first layer and the residual energy deposited in the second layer. He and Li isotopes are well identified in this spectrum. The band corresponding to ^{4}He is prominent, and these particles are completely stopped in the second layer. Specifically, the observation of ^{6}He indicates the occurrence of the 1p-stripping process in the ^{7}Li-induced reaction. In Fig. 5(b), E_2 is the energy loss in the second layer, and E_3 is the residual energy deposited in the third layer. In this spectrum, the hydrogen isotopes p, d, and t are well identified. The d and t particles are completely stopped in the third layer.

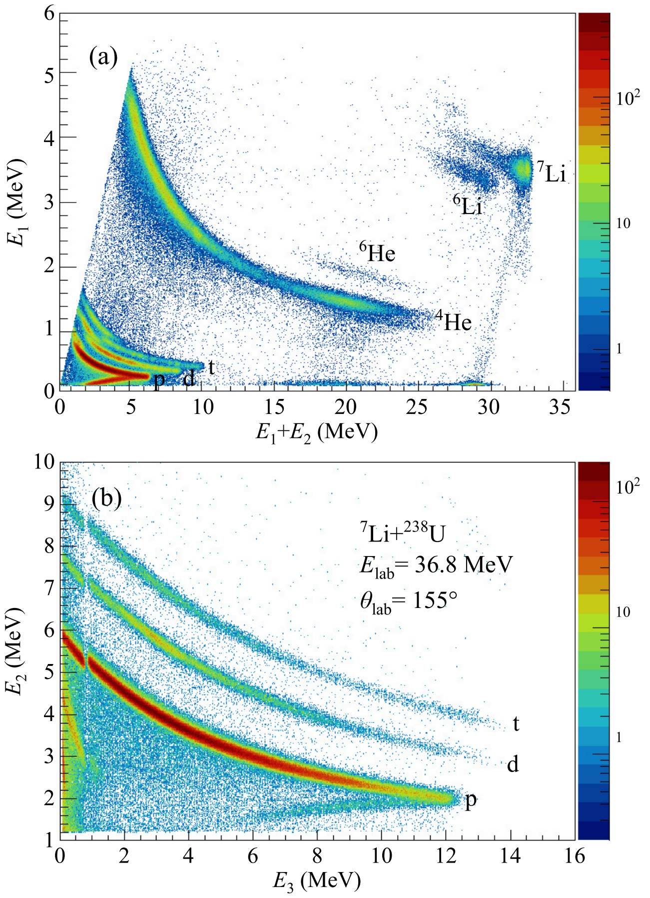

Fig. 5. (Color online) Typical particle identification spectra for light charged particles in ^{7}Li + ^{238}U at $E_{\rm lab}$ = 36.8 MeV and $\theta_{\rm lab}$ = 155°. (a) Identification of the heavier particles using the first and second layers. (b) Identification of the lighter particles using the second and third layers.

C. ^{6}He-gated fission fragment folding angle distribution

The ^{6}He exit channel in the ^{7}Li + ^{238}U system was firstly selected to test the performance of the detector array considering its following advantages: 1) For measurement, the energy loss of scattered ^{7}Li particles in PPAC is small, which reduces the counting rate of PPAC especially in the angular region with small θ relative to the beam direction and hence reduces the dead time for data acquisition. 2) For the emitting channel, the origin of ^{6}He from 1p stripping should be dominant compared to the breakup mechanism due to the large proton separation energy of 9.97 MeV for ^{7}Li. 3) For ^{6}He, it has no bound excitation states, thus avoiding the ambiguity associated with excitation energy partition in the exit channel.

Figure 6 shows a typical correlated energy spectrum of two complementary fission fragments obtained from the cathodes of the two PPACs in ^{7}Li + ^{238}U at $E_{\rm lab}$ = 36.8 MeV, where $E_{\rm F}$ and $E_{\rm B}$ correspond to the energy signals obtained from PPAC$_{\rm F}$ and PPAC$_{\rm B}$, respectively. It can be observed that the heavy fragments produced in the reaction are mainly concentrated in the channel range of 1000-3000. Consequently, the

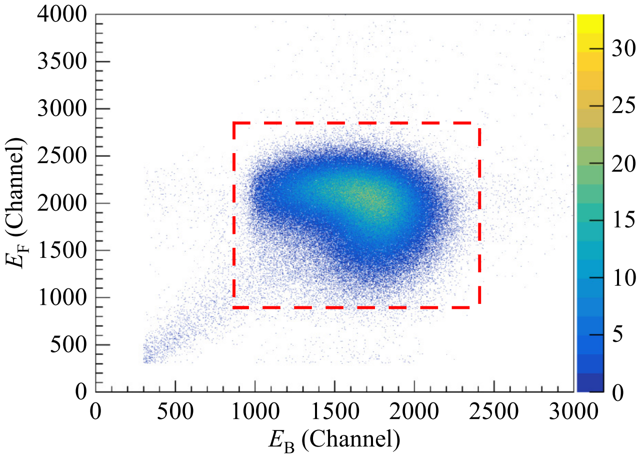

Fig. 6. (Color online) A typical correlated energy spectrum of two complementary fission fragments measured by PPAC$_F$ and PPAC$_B$ in ^{7}Li + ^{238}U at $E_{\rm lab}$ = 36.8 MeV. The red dashed contour indicates the selected fission events used for further analysis.

clean fission events selected for subsequent analysis are enclosed within the red contour.

The folding angle distribution is a sensitive probe to select the non-complete momentum transfer events. The folding angle distribution for all events in which both fission fragments were detected by PPAC$_F$ and PPAC$_B$ in ^{7}Li + ^{238}U at $E_{\rm lab}$ = 36.8 MeV is shown in Fig. 7 as solid circles. These events correspond to the total fission (TF) yield, including both complete-fusion fission and fission following direct reactions. It shows an obvious deviation from a Gaussian shape. A double-Gaussian fitting, shown as the solid line, was used to roughly fit the shape. The main component concentrating at ∼173° agrees with the Viola systematics [52] assuming fission from the complete fusion (CF) with full-momentum transfer. In addition, a pronounced lower angle component centered at ∼168° is observed, corresponding to the non-complete fusion events.

A total of 1790 triple coincidence events of ^{6}He particles with both fission fragments detected by PPAC$_F$ and PPAC$_B$ were obtained, yielding the folding angle distribution shown in Fig. 7 as the solid triangles. It can be seen that the peak position of the ^{6}He correlated fission fragments shows obvious deviation from the peak position of ∼173°. It is roughly reproduced by the single Gaussian fitting with a smaller peak angle compared to the CF, shown as the dash-dotted line in Fig. 7. This is reasonable for a higher recoil velocity of TLP considering that the measured ^{6}He particles emitted in the backward angular region will transfer larger linear momentum to the target nucleus compared to situation in CF events.

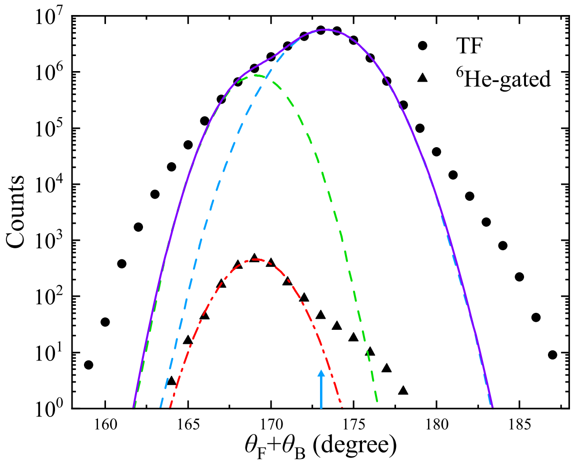

Fig. 7. (Color online) The folding angle distributions of the total fission fragments (solid circles) and ^{6}He-gated fission fragments (solid triangles) obtained in ^{7}Li + ^{238}U at $E_{\rm lab}$ = 36.8 MeV. The double-Gaussian fitting curve is for the total fission, where the higher peak corresponds the CF components in accordance with the arrow position calculated by assuming Viola kinematics [52], and the lower peak corresponds to the non-complete momentum transfer components. The solid line is the summed one. The fitting for ^{6}He-coincident one is shown as the dash-dotted line.

D. Fission probability of ^{239}Np as a function of excitation energy obtained from the ^{238}U(^{7}Li,^{6} He)^{239}Np reaction channel

The fission barrier height corresponds to the excitation energy where the fission probability is half of the maximum of the first-chance fission probability [53]. Experimentally, the method based on the variation of the fission probability with excitation energy has been widely used to obtain the fission barrier height of a nuclide [41, 43, 44, 54].

In the present case, the measured ^{6}He particles can only populate the ground state, so all the excitation energy in the exit channel is imparted to the TLP ^{239}Np. By measuring the energy $E_{\rm b}$ and emission angle θ of ^{6}He, the excitation energy of ^{239}Np can be unambiguously determined by applying the conservation laws of energy and momentum [54]:

$$E^* = Q_{\rm gg} - \frac{E_{\rm a}(M_{\rm a} - M_{\rm B}) - E_{\rm b}(M_{\rm b} + M_{\rm B}) + 2\sqrt{M_{\rm a} M_{\rm b} E_{\rm lab} E_{\rm b}}\cos\theta}{M_{\rm B}}, \tag{1}$$

where a, b and B represent the beam, beam-like and target-like particles, respectively. M_i represents the mass of each nucleus involved in the reaction, $Q_{\rm gg}$ is the Q-value of the transfer reaction populating the ground states for the two emitting particles.

The fission probability $P_{\rm Fis}$, extracted from the double coincidence between the BLP and either FF, is defined as the ratio of the fission cross section $\sigma_{\rm Fis}$ to the reaction cross section σ_{r} for forming the compound nucleus in the specific transfer channel [44, 54]. For PPAC$_{\mathrm{i}}$, the corresponding quantity P^{i}_{Fis} is given by

$$P^{\mathrm{i}}_{\mathrm{Fis}}(E^{*}) = \frac{N_{\mathrm{BLP-FF_{i}}}(E^{*})}{N_{\mathrm{BLP}}(E^{*})\varepsilon_{\mathrm{i}}(E^{*})}, \tag{2}$$

where N_{BLP} is the count of the outgoing beam-like ^{6}He particles detected by the silicon strip detectors, corresponding to TLP events; $N_{\mathrm{BLP-FF_{i}}}$ is the count obtained from coincidence between BLP and any fission fragment detected by either PPAC detector, corresponding to events where the TLPs undergo fission; ε_{i} is the fission detection efficiency defined as [41]

$$\varepsilon_{\mathrm{i}} = \frac{2\Omega_{\mathrm{PPACi}}}{4\pi}, \tag{3}$$

The factor of 2 in the numerator is due to producing two fission fragments in a fission event. This is the so-called geometrical efficiency. This definition has been widely used [41, 43, 44] and confirmed reliable within a deviation of 10%-level recently for ^{243}Am(^{3}He,t)^{243}Cm within an excitation energy range of 5.5-15.0 MeV by comparing with a Monte Carlo simulation result based on a high statistical measurement of the fission fragment angular distribution [54]. In addition, corrections for both the intrinsic efficiency and the random coincidence efficiency ($P^{\mathrm{random}}_{\mathrm{Fis}}$) were applied. The intrinsic efficiency was determined by comparing the number of backward fission fragments identified in coincidence with the forward PPAC within a confined angular region expected to be covered by the backward PPAC, and was found to be approximately 99.6% in the present experiment. $P^{\mathrm{random}}_{\mathrm{Fis}}$ was estimated from the correlation between elastically scattered ^{7}Li particles and fission fragments, for which no real fission is expected, and was found to be approximately 0.01.

The experimentally extracted fission probability P_{Fis} obtained from coincidence with PPAC$_{\mathrm{F}}$ as a function of excitation energy E^{*} for the target-like nucleus ^{239}Np is shown in Fig. 8 as solid circles, where the error bars represent only statistical uncertainties. The measurement covers a wide excitation energy range below 12.5 MeV, and the obtained $P^{\mathrm{max}}_{\mathrm{Fis}}$ is 0.57(4), averaged over all pixels of the silicon detector telescopes. The result obtained from coincidence with PPAC$_{\mathrm{B}}$ is similar, giving $P^{\mathrm{max}}_{\mathrm{Fis}}$ = 0.63(4). A significant discrepancy is observed between the present ($P^{\mathrm{max}}_{\mathrm{Fis}}$) result and the literature value reported by JAEA [44]. The lower value reported by JAEA is attributed to the strong horizontal tail of elastically scattered particles produced in the above-barrier ^{18}O + ^{237}Np reaction, which strongly affects the extraction of the fission probability in the excitation energy region near the fission barrier, as well as to the use of a relatively large 0.8 MeV bin width, resulting from poor energy resolution.

For the fitting to the fission barrier, it should be pointed out that due to the fact that the rising part of the fission probability curve in Fig. 8 contains only a few data points, this limited energy resolution precludes the observation of any resonance (class-II) sub-barrier structures, which are sensitive to both the inner and outer barrier heights [55]. Although actinide nuclei typically exhibit a complex double-humped fission barrier structure, it is well known that the use of a single-humped Hill-Wheeler approximation allows for a consistent derivation of the barrier height corresponding to the higher one determined by the double-humped fission barrier model [56]. The Hill-Wheeler fitting formula is expressed as [57]:

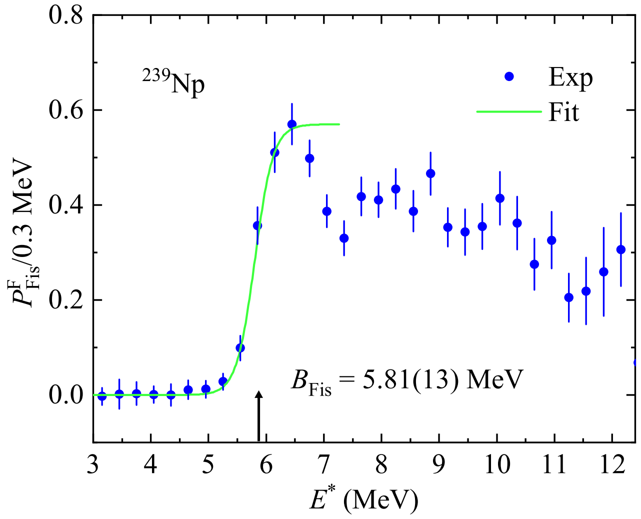

Fig. 8. (Color online) Experimentally extracted fission probability $P^{\mathrm{F}}_{\mathrm{Fis}}$ as a function of the excitation energy E^{*} for ^{239}Np by using the ^{238}U(^{7}Li,^{6}He)^{239}Np at E_{lab} = 36.8 MeV. The solid circles represent the experimental data, and the solid line is the fitting curve by using Eq. 4.

Table 1. The extracted values of $P^{\mathrm{max}}_{\mathrm{Fis}}$ and B_{Fis} for ^{239}Np from ^{238}U(^{7}Li,^{6}He)^{239}Np reaction channel by using coincidence with PPAC$_{\mathrm{F}}$ or PPAC$_{\mathrm{B}}$.

Method	$P^{\mathrm{random}}_{\mathrm{Fis}}$	$P^{\mathrm{max}}_{\mathrm{Fis}}$	B_{Fis}
BLP-FF$_{\mathrm{F}}$	0.01	0.57(4)	5.81(13)
BLP-FF$_{\mathrm{B}}$	0.01	0.63(4)	5.82(12)

$$P_{\mathrm{Fis}}(E^{*}) = \frac{P^{\mathrm{max}}_{\mathrm{Fis}}}{1+\exp\left[\frac{2\pi(B_{\mathrm{Fis}}-E^{*})}{\hbar\omega}\right]}, \tag{4}$$

where $P^{\mathrm{max}}_{\mathrm{Fis}}$, B_{Fis}, and $\hbar\omega$ are adjustable parameters representing the maximum fission probability for the first-chance fission, fission barrier height, and fission barrier curvature, respectively.

Using Eq. 4, the fit was carried out over the sub-barrier and first-chance fission energy region. The fitting result, shown by the green solid curve in Fig. 8, reproduces the rising part of the fission probability curve well, and the extracted fission barrier heights B_{Fis} are listed in Table 1. As shown in the table, the extracted values of $P^{\mathrm{max}}_{\mathrm{Fis}}$ and B_{Fis} are consistent for different fission fragment emission angles. This provides experimental evidence that the effect of angular anisotropy on the extracted results is minor [54].

The comparison of the average value of the extracted fission barrier height 5.82 ± 0.13 MeV for ^{239}Np from this work with the literature data [42–44] is shown in Table 2. It can be

Table 2. The extracted fission barrier heights for ^{239}Np from this work in comparison with the literature data [42–44].

Reaction	$B_{\rm Fis}$ (MeV)	Refs.
^{238}U(^{7}Li,^{6}He)^{239}Np	5.82 ± 0.13	This work
^{237}Np(^{18}O,^{16}O)^{239}Np	5.86 ± 0.09	[44]
^{238}U(^{3}He, d)^{239}Np	5.85 ± 0.30	[42]
^{238}U(^{3}He, d)^{239}Np	5.70 ± 0.20	[43]

seen that the present experimental result is in good consistence with the available data [42–44], validating the feasibility of determining fission barrier heights via transfer-induced fission using the present detector array.

V. SUMMARY

In this work, a hybrid detector array for coincidence measurements of the direct reaction products and the fission fragments has been designed and fabricated. The combination of large-area silicon strip detectors and large-sensitive-area PPAC detectors provides a large solid-angle coverage of 0.95π for the detector array, significantly improving the coincidence detection efficiency and hence enabling the extension to the reaction channels with smaller cross sections.

The present hybrid detector array has been applied to FF-BLP coincidence measurement for the weakly bound ^{7}Li + ^{238}U system at $E_{\rm lab}$ = 36.8 MeV. Benefiting from the good energy and angular resolutions of the silicon strip detectors for ^{6}He, a good excitation energy resolution for the excitation energy of ^{239}Np was obtained. The folding angle distribution gives further support for incomplete momentum transfer in the beam-like ^{6}He emitting channel. Furthermore, the $B_{\rm Fis}$ of ^{239}Np was extracted from the dependence of fission probability on excitation energy. The result is in good agreement with the available results. The reliability of extraction of the fission barrier height based on nucleon transfer reactions induced by light projectiles by using the present setup has been validated. This opens up the possibility of supplementing experimental fission data for more short-lived and highly radioactive actinide nuclides. On the other hand, the quantitative extraction of breakup- or transfer-induced fission in the α- and t- emitting channels by using the obtained data is in progress.

AUTHOR CONTRIBUTIONS

All authors contributed to the study conception and design. Material preparation was performed by C.J. Lin, H.M. Jia, J. Feng, and Y.J. Qiu. Data analysis and the first draft of the manuscript were prepared by S.X. Zhu. All authors commented on previous versions of the manuscript and approved the final version.

REFERENCES

[1] L.F. Canto, P.R.S. Gomes, R. Donangelo et al., Fusion and breakup of weakly bound nuclei, Phys. Rep. **424**, 1-111 (2006). https://doi.org/10.1016/j.physrep.2005.10.006

[2] R. Kaur, B.B. Singh, M. Kaur et al., Investigating ^{6,7}Li-induced reactions on ^{235,238}U through a collective clusterization approach, Phys. Rev. C **108**, 034611 (2023). https://doi.org/10.1103/PhysRevC.108.034611

[3] W.V. Oertzen, M. Freer, Y. Kanada-En'yo, Nuclear clusters and nuclear molecules, Phys. Rep. **432**, 43-113 (2006). https://doi.org/10.1016/j.physrep.2006.07.001

[4] K. Wei, Y.L. Ye, Z.H. Yang, Clustering in nuclei: progress and perspectives, Nucl. Sci. Tech. **35**, 216 (2024). https://doi.org/10.1007/s41365-024-01588-x

[5] Y. Blumenfeld, F. Auger, J.E. Sauvestre et al., MUST: A silicon strip detector array for radioactive beam experiments, Nucl. Instr. Meth. A **421**, 471-491 (1999). https://doi.org/10.1016/S0168-9002(98)01178-4

[6] T. Davinson, W. Bradfield-Smith, S. Cherubini et al., Louvain-Edinburgh Detector Array (LEDA): a silicon detector array for use with radioactive nuclear beams, Nucl. Instr. Meth. A **454**, 350-358 (2000). https://doi.org/10.1016/S0168-9002(00)00479-4

[7] M. Romoli, E. Vardaci, A. Anastasio et al., EXPADES: A new detection system for charged particles in experiments with RIBs, Nucl. Instr. Meth. B **266**, 4637-4642 (2008). https://doi.org/10.1016/j.nimb.2008.05.121

[8] G. Marquínez-Durán, L. Acosta, R. Berjillos et al., GLORIA: A compact detector system for studying heavy ion reactions using radioactive beams, Nucl. Instr. Meth. A **755**, 69-77 (2014). https://doi.org/10.1016/j.nima.2014.04.002

[9] N.R. Ma, L. Yang, C.J. Lin et al., MITA: A Multilayer Ionization-chamber Telescope Array for low-energy reactions with exotic nuclei, Eur. Phys. J. A **55**, 87 (2019). https://doi.org/10.1140/epja/i2019-12765-7

[10] Y.S. Wu, G.L. Zhang, C.J. Lin et al., STARE: a new detector array for exploring the breakup reaction mechanisms induced by weakly bound nuclei, Nucl. Sci. Tech. **36**, 214 (2025). https://doi.org/10.1007/s41365-025-01783-4

[11] L. Yang, C.J. Lin, H.M. Jia et al., Experimental investigations on near-barrier reactions with weakly-bound nuclei at the China Institute of Atomic Energy, Eur. Phys. J. A **61**: 124 (2025). https://doi.org/10.1140/epja/s10050-025-01598-2

[12] V.V. Parkar, S.K. Sharma, R. Palit et al., Investigation of complete and incomplete fusion in the ^{7}Li + ^{124}Sn reaction near Coulomb barrier energies, Phys. Rev. C **97**, 014607 (2018). https://doi.org/10.1103/PhysRevC.97.014607

[13] M. Dasgupta, P.R.S. Gome, D.J. Hinde et al., Effect of breakup on the fusion of ^{6}Li, ^{7}Li, and ^{9}Be with heavy nuclei, Phys. Rev. C **70**, 024606 (2004). https://doi.org/10.1103/PhysRevC.70.024606

[14] L. Jin, A.M. Moro, Unraveling the reaction mechanisms leading to partial fusion of weakly bound nuclei, Phys. Rev. Lett. **123**, 232501 (2019). https://doi.org/10.1103/PhysRevLett.123.232501

[15] K.J. Cook, E.C. Simpson, L.T. Bezzina et al., Origins of Incomplete Fusion Products and the Suppression of Complete Fusion in Reactions of ^{7}Li, Phys. Rev. Lett. **122**, 102501 (2019). https://doi.org/10.1103/PhysRevLett.122.102501

[16] A. Shrivastava, A. Navin, A. Diaz-Torres et al., Role of the cluster structure of ^{7}Li in the dynamics of fragment capture, Phys. Lett. B **718**, 931-936 (2013). https://doi.org/10.1016/j.physletb.2012.11.064

[17] M. Dasgupta, D.J. Hinde, R.D. Butt et al., Fusion versus breakup: Observation of large fusion suppression for ^{9}Be + ^{208}Pb, Phys. Rev. Lett. **82**, 1395 (1999). https://doi.org/10.1103/PhysRevLett.82.1395

[18] D.R. Zolnowski, H. Yamada, S.E. Cala et al., Evidence for "Massive Transfer" in Heavy-Ion Reactions on Rare-Earth Targets, Phys. Rev. Lett. **41**, 92 (1978). https://doi.org/10.1103/PhysRevLett.41.92

[19] S. Bottoni, S. Leoni, B. Fornal et al., Cluster-transfer reactions with radioactive beams: A spectroscopic tool for neutron-rich nuclei, Phys. Rev. C **92**, 024322 (2015). https://doi.org/10.1103/PhysRevC.92.024322

[20] S.K. Pandit, A. Shrivastava, K. Mahata et al., Unraveling the reaction mechanism for large alpha production and incomplete fusion in reactions involving weakly bound stable nuclei, Phys. Lett. B **820**, 136570 (2021). https://doi.org/10.1016/j.physletb.2021.136570

[21] S.K. Pandit, A. Shrivastava, K. Mahata et al., Investigation of large α production in reactions involving weakly bound ^{7}Li, Phys. Rev. C **96**, 044616 (2017). https://doi.org/10.1103/PhysRevC.96.044616

[22] M.K. Pradhan, A. Mukherjee, P. Basu et al., Fusion of ^{6}Li with ^{159}Tb at near-barrier energies, Phys. Rev. C **83**, 064606 (2011). https://doi.org/10.1103/PhysRevC.83.064606

[23] R. Prajapat, M. Maiti, Probing the influence of incomplete fusion in the ^{6}Li + ^{89}Y reaction up to 7.2 MeV/nucleon energy, Phys. Rev. C **103**, 034620 (2021). https://doi.org/10.1103/PhysRevC.103.034620

[24] P.K. Rath, S. Santra, N.L. Singh et al., Complete fusion in ^{7}Li + ^{144,152}Sm reactions, Phys. Rev. C **88**, 044617 (2013). https://doi.org/10.1103/PhysRevC.88.044617

[25] M.L. Wang, G.X. Zhang, S.P. Hu et al., Study on the reaction channels in the ^{6}Li + ^{89}Y system with multi-angular proton and deutron-γ coincidence analysis, Nucl. Phys. A **1049**, 122914 (2024). https://doi.org/10.1016/j.nuclphysa.2024.122914

[26] A. Pal, S. Santra, D. Chattopadhyay et al., Measurement of incomplete fusion cross sections in ^{6,7}Li + ^{238}U reactions, Phys. Rev. C **99**, 024620 (2019). https://doi.org/10.1103/PhysRevC.99.024620

[27] R. Raabe, J.L. Sida, J.L. Charvet et al., No enhancement of fusion probability by the neutron halo of ^{6}He, Nature **431**, 823-826 (2004). https://doi.org/10.1038/nature02984

[28] R. Raabe, C. Angulo, J.L. Charvet et al., Fusion and direct reactions around the barrier for the systems ^{7,9}Be, ^{7}Li + ^{238}U, Phys. Rev. C **74**, 044606 (2006). https://doi.org/10.1103/PhysRevC.74.044606

[29] K.H. Schmidt, B. Jurado, Review on the progress in nuclear fission—experimental methods and theoretical descriptions, Rep. Prog. Phys. **81**, 106301 (2018). https://doi.org/10.1088/1361-6633/aacfa7

[30] A.N. Andreyev, K. Nishio, K.H. Schmidt, Nuclear fission: a review of experimental advances and phenomenology, Rep. Prog. Phys. **81**, 016301 (2018). https://doi.org/10.1088/1361-6633/aa82eb

[31] A. Chatillon, J. Taïeb, H. Alvarez-Pol et al., Experimental study of nuclear fission along the thorium isotopic chain: From asymmetric to symmetric fission, Phys. Rev. C **99**, 054628 (2019). https://doi.org/10.1103/PhysRevC.99.054628

[32] A. Bulgac, S. Jin, I. Stetcu, Nuclear fission dynamics: Past, present, needs, and future, Front. Phys. **8**, 63 (2020). https://doi.org/10.3389/fphy.2020.00063

[33] M. Bender, R. Bernard, G. Bertsch et al., Future of nuclear fission theory, J. Phys. G: Nucl. Part. Phys. **47**, 113002 (2020). https://doi.org/10.1088/1361-6471/abab4f

[34] M.D. Mathew, Nuclear energy: A pathway towards mitigation of global warming, Prog. Nucl. Energy **143**, 104080 (2022). https://doi.org/10.1016/j.pnucene.2021.104080

[35] M. Eichler, A. Arcones, A. Kelic et al., The role of fission in neutron star mergers and its impact on the r-process peaks, Astrophys. J. **808**, 30 (2015). https://doi.org/10.1088/0004-637X/808/1/30

[36] N. Bohr, J.A. Wheeler, The Mechanism of Nuclear Fission, Phys. Rev. **56**, 426 (1939). https://doi.org/10.1103/PhysRev.56.426

[37] H.C. Britt, J.D. Cramer, Fission-Fragment Angular Correlations for ^{233}U, ^{235}U, and ^{239}Pu (t, df) Reactions, Phys. Rev. **181**, 1634 (1969). https://doi.org/10.1103/PhysRev.181.1634

[38] J.A. Northrop, R.H. Stokes, K. Boyer, Measurement of the Fission Thresholds of ^{239}Pu, ^{233}U, ^{235}U, and ^{238}U Using the (d, p) Reaction, Phys. Rev. **115**, 1277 (1959). https://doi.org/10.1103/PhysRev.115.1277

[39] Q. Ducasse, B. Jurado, M. Aïche et al., Investigation of the ^{238}U(d, p) surrogate reaction via the simultaneous measurement of γ-decay and fission probabilities, Phys. Rev. C **94**, 024614 (2016). https://doi.org/10.1103/PhysRevC.94.024614

[40] P. Glässel, H. Rösler, H.J. Specht, Intermediate structure in the ^{239}Pu(d, pf) reaction, Nucl. Phys. A **256**, 220-242 (1976). https://doi.org/10.1016/0375-9474(76)90105-6

[41] B.B. Back, O. Hansen, H.C. Britt et al., Fission of doubly even actinide nuclei induced by direct reactions, Phys. Rev. C **9**, 1924 (1974). https://doi.org/10.1103/PhysRevC.9.1924

[42] B.B. Back, H.C. Britt, O. Hansen et al., Fission of odd-A and doubly odd actinide nuclei induced by direct reactions, Phys. Rev. C **10**, 1948 (1974). https://doi.org/10.1103/PhysRevC.10.1948

[43] A. Gavron, H.C. Britt, E. Konecny et al., Γ_n/Γ_f for actinide nuclei using (^{3}He, df) and (^{3}He, tf) reactions, Phys. Rev. C **13**, 2374 (1976). https://doi.org/10.1103/PhysRevC.13.2374

[44] K.R. Kean, K. Nishio, K. Hirose et al., Validation of the multinucleon transfer method for the determination of the fission barrier height, Phys. Rev. C **100**, 014611 (2019). https://doi.org/10.1103/PhysRevC.100.014611

[45] Micron Semiconductor Ltd., Royal Bldg, Marlborough Rd. Lancing, Sussex, UK BN15 8UN, private communication.

[46] D.X. Wang, C.J. Lin, L. Yang et al., Compact 16-channel integrated charge-sensitive preamplifier module for silicon strip detectors, Nucl. Sci. Tech. **31**, 48 (2020). https://doi.org/10.1007/s41365-020-00755-0

[47] H.M. Jia, C.J. Lin, B. Paes et al., No sub-Coulomb-barrier fusion enhancement due to positive Q-value two-neutron stripping: The ^{18}O + ^{58}Ni case, Phys. Rev. C **111**, 034606 (2025). https://doi.org/10.1103/PhysRevC.111.034606

[48] H.R. Wang, C.J. Lin, N.R. Ma et al., The heavy-ion time-of-flight spectrometer HiToF, Nucl. Sci. Tech. **36**, 53 (2025). https://doi.org/10.1007/s41365-025-01819-9

[49] L. Yang, C.J. Lin, H.M. Jia et al., Optical model potentials for ^{6}He + ^{64}Zn from ^{63}Cu(^{7}Li, ^{6}He)^{64}Zn

reactions, Phys. Rev. C **95**, 034616 (2017). https://doi.org/10.1103/PhysRevC.95.034616

[50] L. Yang, C.J. Lin, H.M. Jia et al., Is the Dispersion Relation Applicable for Exotic Nuclear Systems? The Abnormal Threshold Anomaly in the ^{6}He + ^{209}Bi System, Phys. Rev. Lett. **119**, 042503 (2017). https://doi.org/10.1103/PhysRevLett.119.042503

[51] X.L. Wei, F.H. Guan, H.R. Yang, et al., Development of Parallel Plate Avalanche Counter for heavy ion collision in radioactive ion beam, Nucl. Eng. Technol. **52**, 575 (2020). https://doi.org/10.1016/j.net.2019.08.020

[52] V.E. Viola, K. Kwiatkowski, M. Walker, Systematics of fission fragment total kinetic energy release, Phys. Rev. C **31**, 1550 (1985). https://doi.org/10.1103/PhysRevC.31.1550

[53] R. Vandenbosch, J.R. Huizenga, *Nuclear Fission* (Academic, New York, 1973), p. 227.

[54] G. Kessedjian, B. Jurado, G. Barreau et al., Fission probabilities of $^{242}\mathrm{Am}$, $^{243}\mathrm{Cm}$, and $^{244}\mathrm{Cm}$ induced by transfer reactions, Phys. Rev. C **91**, 044607 (2015). https://doi.org/10.1103/PhysRevC.91.044607

[55] S. Bjϕrnholm, J.E. Lynn, The double-humped fission barrier. Rev. Mod. Phys. **52**, 725 (1980). https://doi.org/10.1103/RevModPhys.52.725

[56] J.D. Cramer, J.R. Nix, Exact Calculation of the Penetrability Through Two-Peaked Fission Barriers, Phys. Rev. C **2**, 1048 (1970). https://doi.org/10.1103/PhysRevC.2.1048

[57] D.L. Hill J.A. Wheeler, Nuclear Constitution and the Interpretation of Fission Phenomena, Phys. Rev. **89**, 1102 (1953). https://doi.org/10.1103/PhysRev.89.1102